arXiv:1704.01181v1 [physics.plasm-ph] 4 Apr 2017

An extremely high charge electron accelerator from high power laser-solid interaction

Yong Ma[1,8], Jiarui Zhao[1], Yifei Li[1], Dazhang Li[5], Liming Chen[1,2,3,4,*], Jianxun Liu[6], Yanyun Ma[6,†], Xiaohu Yang[6], Zheyi Ge[6], Zhengming Sheng[2,3,7], and Jie Zhang[2,3‡]

[1] *Beijing National Laboratory of Condensed Matter Physics, Institute of Physics, CAS, Beijing 100190, China*

[2] *IFSA Collaborative Innovation Center, Shanghai Jiao Tong University, Shanghai 200240, China*

[3] *Department of Physics and Astronomy, Shanghai Jiao Tong University, Shanghai 200240, China*

[4] *School of Physical Sciences, University of Chinese Academy of Sciences, Beijing 100049, China*

[5] *Institute of High Energy Physics, CAS, Beijing 100049, China*

[6] *College of Science, National University of Defense Technology, Changsha 410073, China*

[7] *Department of Physics, Scottish Universities Physics Alliance, University of Strathclyde, Glasgow G4 0NG, United Kingdom and*

[8] *Department of Physics, Lancaster University, Bailrigg, LA1 4YW, United Kingdom*

Compact acceleration of tightly collimated relativistic electron beam with high charge from laser-plasma interaction has many unique applications. However, currently the well-known schemes including laser wakefield acceleration from gas and vacuum laser acceleration from solid often produce electron beams either with low charge or with large divergence angles, suffering from lack of balance between the plasma density and the collimation force. In this work, we report the generation of well collimated electron beams with the divergence angle of a few degrees, quasi-monoenergetic spectra peaked at the MeV-level, and extremely high charge (∼100 nC) via the powerful sub-ps laser pulse interacting with solid target. Particle-in-cell simulations illustrate a new direct laser acceleration scenario. The laser pulse is found to develop self-filamentation in large-scale near-critical density pre-plasma, during which plenty of electron bunches are accelerated periodically and collimated by self-generated magnetic field. Such high charge beams are suitable for broad applications such as single shot electron radiography, ultrafast pump-probe of matter, and ultra-intense γ-ray sources.

INTRODUCTION

In the studies of laser-plasma acceleration (LPA), several laser wakefield accelerator concepts (LWFA) [1], including plasma beat wave accelerator[1, 2], self-modulated laser wakefield accelerator (SM-LWFA) [3], cross-modulated laser wakefield accelerator [4] and LWFA in the bubble regime [5, 6], have been proposed in the last few decades. The successful generation of high quality electron beams at GeV scale with quasi-monoenergetic spectra prospers the study of laser-plasma accelerators worldwide [7–14]. However, almost all the LPA experiments and the theoretical models are based on the interaction between laser and gases, limiting the beam charge to typically few tens pC. While the charge of the electron bunch could reach to few nC in laser-solid interaction due to much higher absorption efficiency and attempts have been made to optimize beam collimation [15–22], the beam quality still need to be greatly improved due to their large divergence angles and quasi-thermal broad energy spectra. Such electron beams are usually generated via several mechanisms such as resonant absorption [23], vacuum heating [24, 25], J×B heating [26], stochastic heating [27] which result in the unsatisfied beam quality. Directional electron beams with nC scale beam charge were produced via vacuum laser acceleration (VLA) with a plasma mirror injector [28]. Unfortunately, the beam collimation also suffers from the pondermotive force of the laser pulse in vacuum during acceleration, which results in a large divergence angle (hundreds mrads) and a halo in the electron beam profile. Recently, few MeV quasi-monoenergetic electron acceleration has been observed in fs laser-solid interaction with beam divergence angle of $1-2^o$ [29]. However, the beam charge is still limited in hundreds pC, and the underlying physics of such acceleration remains unclear.

In this paper, electron beams with extremely high beam charge of approximately 100 nC were generated for the first time in 200 TW, sub-ps laser-solid interaction with deliberately induced pre-plasma. The electron beams are highly collimated with average divergence angle smaller than 3^o and the energy spectra are quasi-monoenergetic with peaks at several MeV. PIC simulations illustrate a new scenario of electron acceleration in which the acceleration and the confinement regimes were combined in a unique way. It is shown that electron beams are mainly produced via direct laser acceleration (DLA) [30–36] in plasma channels [37, 38] driven by the long laser pulse in large scale near-critical pre-plasma. The strong self-generated magnetic field in the plasma channel confines the electron beams tightly to preserve the collimation of the beam. The significant improvement of the beam charge benefits from the direct energy transition from laser pulse into electron beams during the DLA process.

EXPERIMENTAL RESULTS

The experiment was performed on Titan at the Jupiter Laser Facility at Lawrence Livermore National Laboratory (LLNL). The setup of the experiment is shown in

* lmchen@iphy.ac.cn
† yanyunma@126.com
‡ jzhang1@sjtu.edu.cn

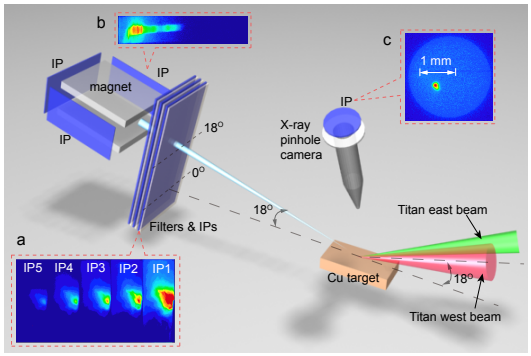

FIG. 1. Experimental set up. Inset figures present (a) the angular distribution of the electron beam on image plates; (b) the energy distribution after deflected by the spectrometer; (c) the image of the X-ray source detected by an X-ray pinhole camera.

Fig. 1 (see **METHOD** for details). Copper block targets were irradiated by a 200 TW, sub-ps laser at an incident angle of 72 in P-polarization. The laser pedestal 3 ns prior to the main pulse (pre-pulse) was measured to be 52 mJ at 1ω with full laser energy of 150 J and 0.2 μJ at 2ω with full laser energy of 35 J, respectively.

Highly collimated and oriented electron bunches with extremely high beam charge were generated, as shown in Fig. 2a, using the full energy laser pulse with approximately 5 mJ pre-pulse. These beams emit along the laser specular reflection direction with an average divergence angle of 2.7^o in FWHM, which is much smaller than those generated via VLA mechanism in laser-solid interaction but similar to the case of laser-driven wakefield accelerator from gas. The beam charge can be as high as 94 nC with energy above 1.0 MeV (see Fig. 2a-III and Fig. 3a). To our best knowledge, this is the first time to observe such high charge electron bunch with such small divergence angle in any case. The beam current reaches $I \simeq 134$ kA by assuming the pulse length of the electron beam is the same with that of the laser pulse. While the Alfv́en current limit [39, 40] in this case is $I_A = 1.65 \times 17[\mathrm{kA}]\sqrt{\gamma^2-1} = 262$ kA, where $\gamma = 9.4$ for the average energy of 5.3 MeV, as shown in Fig. 4c. In addition to the generation of the collimated beams (the central bright spot) in the laser specular direction, a weak plateau appears between laser specular and target normal. This indicates that the generation mechanism of the plateau electrons differs from that of the central bright spot and the energy of such electrons could be much lower. The outgoing direction of plateau electrons is energy dependent with the expression of $sin\alpha' = (\gamma - 1/\gamma)sin\alpha$ [41], where γ is the Lorenz factor of electrons, α' and α are angles between outgoing and laser specular direction with the target normal, respectively.

When increasing the pre-pulse energy to few tens mJ, the electron beam divergence increases a lot but with a similar level of beam charge, as shown in Fig. 2b and

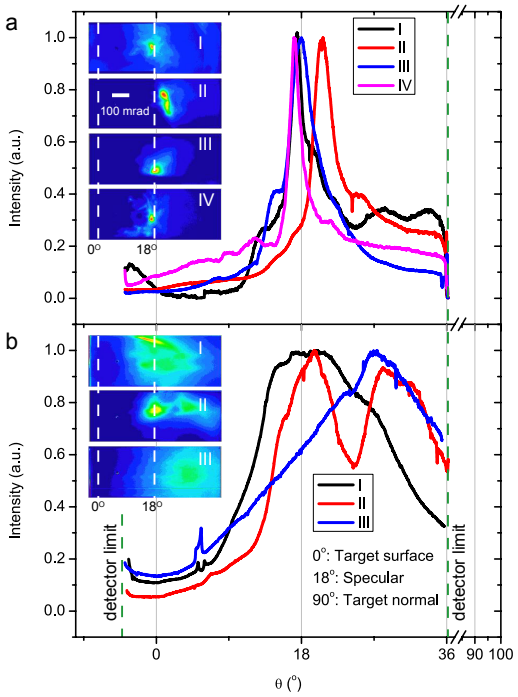

FIG. 2. Angular distribution of the electron beams with 1ω laser pulse. Pre-pulse energy in a(I-IV) are 7, 5, 7, 4 mJ, respectively; Pre-pulse energy in b(I-III) are 20, 32, 82 mJ, respectively.

Fig. 3a. In this case, the outgoing direction of most electrons is between the laser specular and the target normal. Note that the peak intensity of the 5 mJ pre-pulse reaches to $9 \times 10^{15}\mathrm{W/cm^2}$, which is already high enough to produce pre-plasma on solid target. It seems that the pre-plasma scale length has an adverse effect on the beam collimation, while not on the beam charge.

To further investigate the influence of the pre-plasma, we also need to gradually reduce the pre-pulse energy, hence the pre-pulse intensity. However, the 5 mJ pre-pulse is the smallest which can be achieved in case of 1ω. Therefore, second harmonic (2ω) were used in experiment, lowering the pre-pulse energy to 0.2 μJ with intensity below ionization threshold and the main pulse energy to 305 J at the same time. An additional ns laser pulse (Titan east beam in Fig. 1) was used as pre-pulse to produce pre-plasma. The dependence of the electron beam divergence angle and the beam charge on the pre-pulse (Titan east beam) were given in Fig. 3b. Before the introduction of the pre-pulse, i.e., using the 2ω Titan west beam only, the outgoing direction of the electron beams is still along laser specular and the average divergence angle slightly increase to 4.7 due to a relative lower electron energy. However, the beam charge decrease dramatically to an average of only 3 nC. Then, increasing the energy of the pre-pulse gradually and keep the main pulse energy fixed at 305 J, the average FWHM divergence angle of the electron beams increase significantly to 46.4°, while the beam charge remains the same level

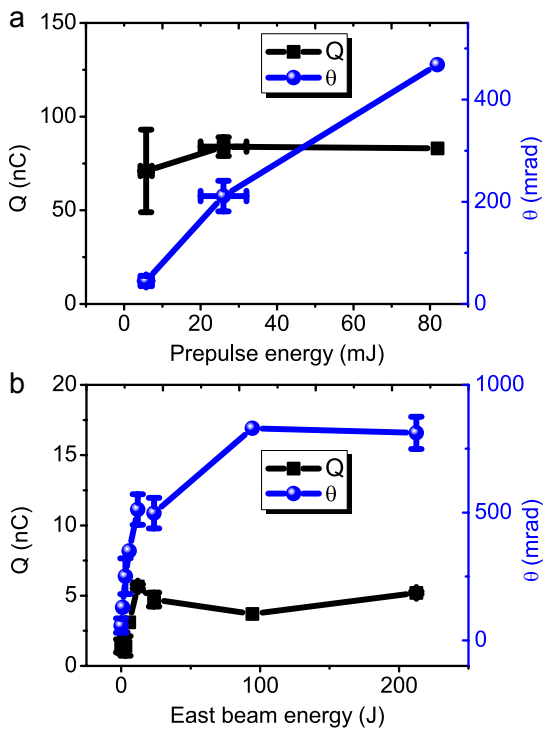

FIG. 3. Electron beam charge and divergence angle. Dependence of electron beam charge and divergence angle on (a) the intrinsic pre-pulse energy of the 1ω main pulse, (b) pre-pulse (Titan east beam) energy with 2ω main pulse.

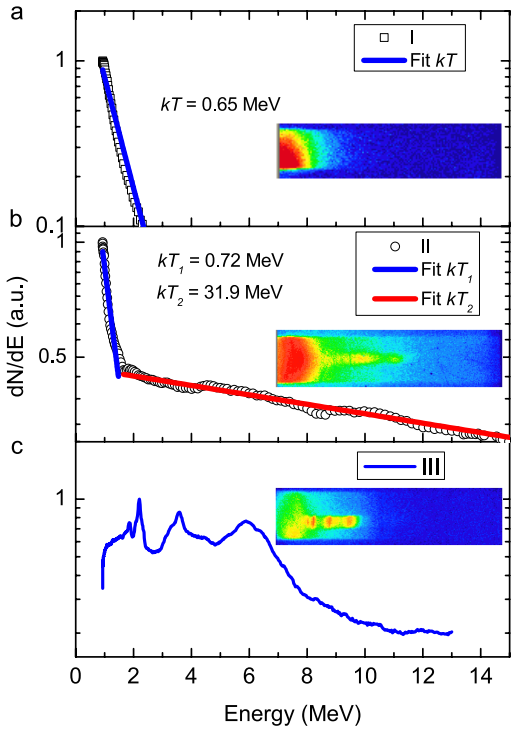

FIG. 4. Energy spectra. Energy spectra of the electron beams with different laser parameters (a) High contrast 2ω; (b) 1ω with high intrinsic pre-pulse energy; (c) 1ω with low intrinsic pre-pulse energy.

(1.4-5.6 nC in average), similar trend with the results in Fig. 3a. Above all, we conclude that main pulse energy plays the key role in controlling the electron beam charge.

The energy spectra of the out-going electron beams are obtained, as shown in Fig. 4. In Fig. 4a, with the 2ω laser pulse and no pre-plasma, most of the electrons are low energy (<1 MeV) and the exponential decay fitting gives an effective temperature $kT = 0.65$ MeV; While in the case of 1ω laser pulse with high pre-pulse, the energy spectrum in Fig. 4b demonstrates obvious dual-temperature distribution. Although the energy of the majority still below 1 MeV with an effective temperature of $kT_1 = 0.72$ MeV, the high-energy tail reaches to 20 MeV with a much higher effective temperature of $kT_2 = 31.9$ MeV. It is obviously that these two groups of electrons with different temperatures have been generated via different mechanism. Low temperature electrons might be produced during laser heating process, such as resonant absorption, J×B heating and so on. While the generation of high temperature electrons could be a result of particular acceleration. As lowering the pre-pulse energy of the 1ω laser pulse to 5 mJ, which is the same condition of Fig. 2a where collimated electron beams with extremely high beam charge, the spectrum becomes quasi-monoenergetic with peaks at 2-6 MeV and the amount of the electrons with lower energy was suppressed, as shown in Fig. 4c.

SIMULATIONS AND DISCUSSION

To further investigate the physics mechanism of the generation of such kind of collimated electron beams with monoenergetic spectra and extremely high beam charge, PIC simulations (see **METHOD**) have been performed and the results agree with that of the experiment quantitatively.

PIC simulation results are shown in Fig. 5. When the main pulse impinges on the target with a large angle in large-scale underdense plasma, it breaks up into several filaments in the pre-plasma produced by the pre-pulse, as shown in Fig. 5c. As the pre-plasma gets denser, each filament is reflected independently. With proper laser intensity and plasma density, the reflected laser filament could drive bubble-like plasma channel, as shown in Figs. 5a and 5b. Fig. 5b illustrates the fine structure of the electron bunches in the plasma channel. It is obviously that the periodic electron bunches with constant spatial distance of half laser wavelength are confined in the bubble-like plasma channel. This spatial distance between electron bunches is a clear evidence of the DLA [30, 34, 35]. The DLA regime was further confirmed by examining the momentum evolution of the accelerated electrons. Fig. 5e illustrates both the longitudinal and transverse momentum evolution of an accelerated elec-

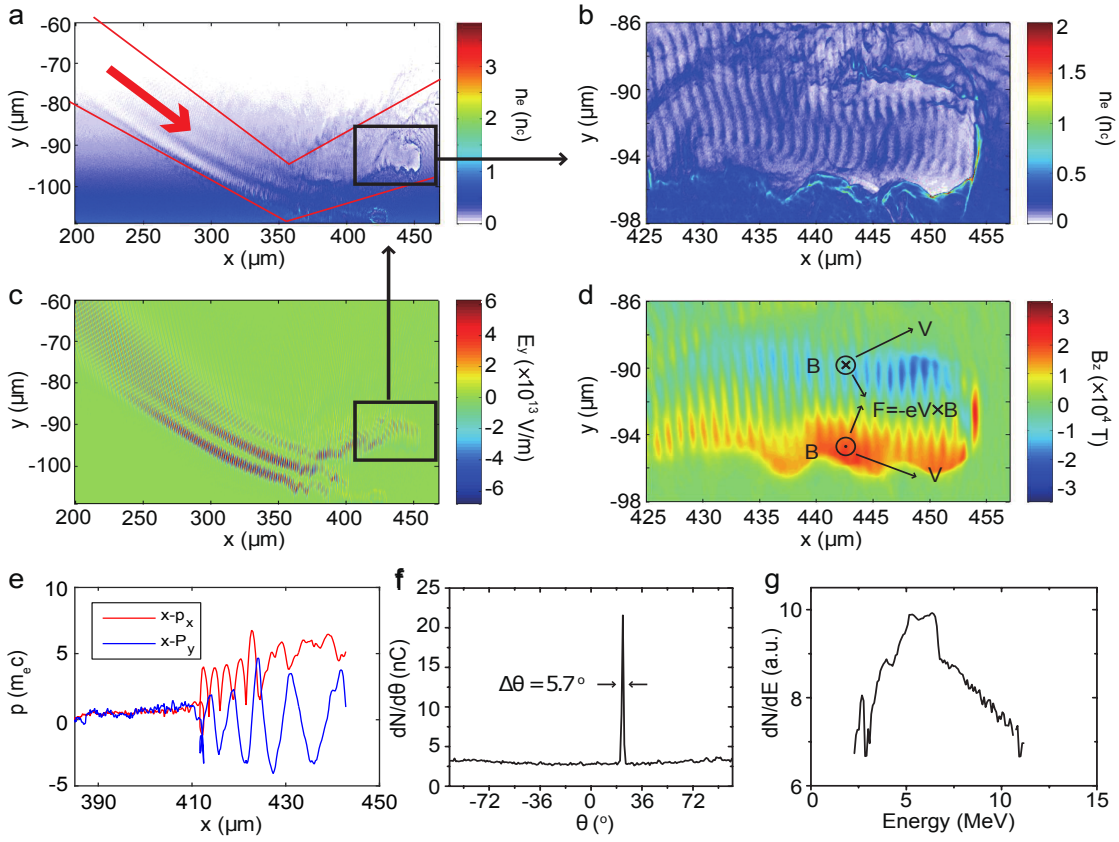

FIG. 5. Simulation results. (a) Electron density distribution at t=490 T_0, (b) Fine structure of electron density in the bubble-like plasma channel. (c) Distribution of laser field Ey. (d) Distribution of magnetic field in the plasma channel. (e) Momenta evolution of an accelerated electron. The angular distribution (f) and the energy spectrum (g) of the electron beams extracted in the region of 500 μm $< x <$ 700 μm and -10 μm $< y <$ 30 μm at t=490 T_0, respectively.

tron, where the oscillation frequency of the longitudinal momentum is twice of that of the transverse momentum, which indicates the well-known "figure 8" motion of the electron in relativistic laser field [42]. In fact, some electrons could gain energy even faster as betatron resonance occurs when the betatron frequency $\omega_\beta = \omega_p/\sqrt{2\gamma}$ equals to the Doppler shifted laser frequency witnessed by the co-moving electrons $\omega = \omega_0\sqrt{(1-\beta)/(1+\beta)}$ [30], where $\omega_p = \sqrt{n_e e^2/\epsilon_0 m_e}$ is the plasma frequency, ω_0 is the laser frequency, $\beta = v/c$.

In the mechanism of VLA, during the direct interaction with the laser field, electrons will escape the focal volume transversely if gaining enough transverse momentum, leading to the large divergence angle of the beam. Besides, the transverse pondermotive force also tends to expel electrons from the laser axis and leads to the formation of the hollow structure in the profile of the electron beams, as observed in Ref. [19, 20, 28] On contrary, the electron beams in our experiment are tightly collimated with small divergence angle $\sim 2.7^o$ and without the hollow structure. As shown in Fig. 5d, strong quasi-static magnetic field with $B \sim 10^4$ T is self-generated in the bubble-like plasma channel due to the strong current driven by massive energetic electrons. The Lorenz force $F_B = -eVB$ tends to prevent electrons from escaping. The strength of the Lorenz force would be higher than that of the laser electric field $F_E = -eE$, considering that the electron velocity vc as $\gamma \gg 1$ and $E_y \sim 10^{12}$V/m in the plasma channel. Similar phenomena are also found in Ref. [43]. On the other hand, the transverse charge separation field of the bubble-like plasma channel would also impose electrons with a focusing force in a similar way with that in the bubble regime of LWFA [44]. As a result, the FWHM divergence angle of the electron beam in simulation is 5.7° (in Fig. 5f) close to our experimental observations. Compared with the results in Ref. [28], although electrons are also directly accelerated in the laser field, the electron beam in our case is tightly confined in a much smaller cone due to the present of the bubble-like plasma channel.

Such DLA in denser plasma channel from solid is different with the LWFA in gas, especially the so-called bubble regime in which the acceleration is mainly occurs in the first wave bucket. In LWFA, the beam charge is limited to few hundreds pC due to the beam-loading effects which ascribe to $Q \propto (k_p R_b)^4/\sqrt{n_e}$ [45] , where R_b is

the bubble radius. We believe this is the reason of the low beam charge in Ref. [29]. While in the DLA, without the limitation of beam-loading, a separate bunch of electrons will be driven in each half optical cycle, leading to much higher beam charge. The comparably long laser pulse duration results in the continuous energy supplement during interaction and guarantees the continuous acceleration process, and this is in accordance with the experimental result that the beam charge increases as the laser energy increase. The total charge of a collimated electron beam in the simulation reaches 126 nC with energy higher 1 MeV, which agrees well with that of the experiment.

Finally, the energy distribution of the electron beam in simulation also agrees with that of the experiment. Fig. 5g gives the energy spectrum of the electron beam which is quasi-monoenergetic with a peak around 6 MeV.

CONCLUSIONS

In conclusion, by using 200 TW sub-picosecond laser pulses, tightly collimated (divergence angle 2.7°), directional and quasi-monoenergetic MeV electron beams with extremely high beam charge (100 nC scale) are generated in experiment for the first time. We have found that the generation of such kind of electron beams is dependent on the laser contrast and the laser energy. PIC simulations illustrate a new electron acceleration scenario in laser-solid interaction. As laser pulse propagates in the near-critical pre-plasma, the self-focusing and filamentation process drives the formation of bubble-like plasma channel, which confines the laser filament itself. Electrons are accelerated via DLA and confined in a small cone mainly due to the focusing Lorenz force induced by the strong self-generated magnetic field. Via DLA, the energy transfer from laser pulse into electron beams boost the beam charge significantly in the case of long pulse duration. Such high charge electron accelerator might find wider applications in seeding high flux ($\sim 2 \times 10^{11}$photons/ps) γ-ray sources, ultrafast probing the warm dense matter, single shot radiography and even in the fast ignition (FI) concept [46].

METHOD

Laser system. The experiment was performed on Titan at the Jupiter Laser Facility at Lawrence Livermore National Laboratory (LLNL). Titan is a two-arm system with a sub-ps west beam and a ns east beam. The wavelength of both arms is 1053 nm. The west beam, as the main pulse, with total energy of 150 J in 700 fs full-width at half maximum (FWHM) pulse duration, was focused by an f/3.5 off-axis parabola to a 7 μm $1/e^2$ spot size, resulting in a laser intensity of 2.8×10^{20}W/cm^2 (a_0=15). The laser pedestal measured at 3 ns prior to the main pulse, i.e., intrinsic pre-pulse, was 52 mJ. By using a KDP crystal to generate second harmonic, the pre-pulse energy can be lower to only 0.2 μJ, while the maximum energy of the main pulse reduces to 35 J. The east beam, which was used as an additional pre-pulse when the main pulse was at 2ω, with maximum energy at 2ω of 220 J in 1 ns FWHM pulse duration, was focused by an f/3.5 lens to a 38 μm $1/e^2$ spot size, resulting in a laser intensity of 1×10^{16}W/cm^2. The time delay of the main pulse to the pre-pulse in this case is 5 ns.

Diagnostics of the electron beams and the X-ray. The angular distribution of the generated electron beams were measured by a couple of image plates (IP, model Fujifilm BAS-SR 2040) as well as the measurement of the beam charge [47]. There are copper filters with thickness of 0.3-1 mm in front of each IP to provide the ability to measure the angular distribution with different energy range in a single shot. To avoid the overestimation of the beam charge due to the generation of hard X-ray photons when the electrons penetrating the metallic filters, simulations were performed by using the Monte Carlo N-particle transport code (MCNP) [48] to calculate the average number of photons generated by electrons. The parameters of the target and the electron beam in the simulations are similar with that of the experiment. We found out that the average number of photons generated is 0.32/electron and the overall PSL contribution ratio from photons to electrons is only $\sim$ 1.6% due to a much smaller sensitivity of the IP to photons, as one can see in Ref. [47] for electrons and Ref. [49] for photons. Therefore, the photons generated when the electron penetrating the filter can be neglected. More detailed MCNP simulation results can be found in the supplemental information. The energy spectra of the electron beams were measured by a spectrometer with magnetic field strength of 9000 G and energy detection range of 0.9-49.4 MeV which is set behind the IPs. An X-ray pinhole camera with magnification of M = 16 was used to measure the size of the plasma region.

Simulations. The simulation has been performed by using the 2D3V PIC code EPOCH [50]on the TianHe Super computer. The pulse duration of the incident laser is 700 fs (FWHM) with a spot size of 7 μm. The wavelength, incident angle and polarization of the laser are the same as that in experiments. The peak intensity of the laser is 2.8×10^{20}W/cm^2. The target is initially located between $y = -110$ μm and $y = -10$ μm with density profile $n_e = 10^{-(y+110)/25} n_c$in the y direction, where $n_c = \epsilon_0 m_e \omega_0^2 / e^2$ is the critical density. The density profile is given by the radiation hydrodynamic code MULTI [51] by assuming that the contrast ratio of the pre-pulse with the main pulse is 10^{-6}. The simulation box size is $x \times y$ = 700×140 μm with 14000×2800 cells. Each cell contains 42 numerical macroparticles per species in the simulations.

AUTHOR CONTRIBUTIONS. L. M. C. designed research; Y. M., L. M. C., J. R. Z., Y. F. L. and D. Z. L. performed experiment; J. X. L., Y. M., Y. Y. M., X. H. Y., Z. Y. G performed the PIC simulations; Y. M.,

L. M. C., J. R. Z. and Y. F. L. analyzed data; Y. M., L. M. C. and Z. M. S. wrote the paper. J. Z. supported the whole project.

ACKNOWLEDGMENTS. We thank Jupiter Laser Facility staffs at Lawrence Livermore National Laboratory (LLNL) for laser and technical support and Dr. Joseph Nilsen for facilitating the experiment. This work was supported by the National Basic Research Program of China (2013CBA01500), National Key Scientific Instrument and Equipment Development Project (2012YQ120047), National Natural Science Foundation of China (11334013,11421064,11374210), the CAS key program (KGZD-EW-T05), the MOST International Collaboration (2014DFG02330), a Leverhulme Trust Research Project Grant, and the U.K. EPSRC grant EP/N028694/1. The EPOCH code was developed as part of the UK EPSRC grants EP/G056803/1 and EP/G055165/1.

[1] T. Tajima and J. M. Dawson, Phys. Rev. Lett. **43**, 267 (1979).
[2] M. N. Rosenbluth and C. S. Liu, Phys. Rev. Lett. **29**, 701 (1972).
[3] J. Krall, A. Ting, E. Esarey, and P. Sprangle, Phys. Rev. E **48**, 2157 (1993).
[4] Z. Sheng, K. Mima, Y. Sentoku, K. Nishihara, and J. Zhang, Physics of Plasmas **9**, 3147 (2002).
[5] A. Pukhov and J. Meyer-ter Vehn, Applied Physics B **74**, 355 (2002).
[6] I. Kostyukov, A. Pukhov, and S. Kiselev, Physics of Plasmas **11**, 5256 (2004).
[7] S. Mangles, C. Murphy, Z. Najmudin, A. Thomas, J. Collier, A. Dangor, E. Divall, P. Foster, J. Gallacher, C. Hooker, D. Jaroszynski, A. Langley, W. Mori, P. Norreys, F. Tsung, R. Viskup, B. Walton, and K. Krushelnick, Nature **431**, 535 (2004).
[8] C. Geddes, C. Toth, J. van Tilborg, E. Esarey, C. Schroeder, D. Bruhwiler, C. Nieter, J. Cary, and W. Leemans, Nature **431**, 538 (2004).
[9] J. Faure, Y. Glinec, A. Pukhov, S. Kiselev, S. Gordienko, E. Lefebvre, J. Rousseau, F. Burgy, and V. Malka, Nature **431**, 541 (2004).
[10] W. P. Leemans, B. Nagler, A. J. Gonsalves, C. Toth, K. Nakamura, C. G. R. Geddes, E. Esarey, C. B. Schroeder, and S. M. Hooker, Nature Physics **2**, 696 (2006).
[11] N. A. M. Hafz, T. M. Jeong, I. W. Choi, S. K. Lee, K. H. Pae, V. V. Kulagin, J. H. Sung, T. J. Yu, K.-H. Hong, T. Hosokai, J. R. Cary, D.-K. Ko, and J. Lee, Nature Photonics **2**, 571 (2008).
[12] X. Wang, R. Zgadzaj, N. Fazel, Z. Li, S. A. Yi, X. Zhang, W. Henderson, Y. Y. Chang, R. Korzekwa, H. E. Tsai, C. H. Pai, H. Quevedo, G. Dyer, E. Gaul, M. Martinez, A. C. Bernstein, T. Borger, M. Spinks, M. Donovan, V. Khudik, G. Shvets, T. Ditmire, and M. C. Downer, Nature Communications **4**, 1988 (2013).
[13] H. T. Kim, K. H. Pae, H. J. Cha, I. J. Kim, T. J. Yu, J. H. Sung, S. K. Lee, T. M. Jeong, and J. Lee, Phys. Rev. Lett. **111**, 165002 (2013).
[14] W. P. Leemans, A. J. Gonsalves, H.-S. Mao, K. Nakamura, C. Benedetti, C. B. Schroeder, C. Tóth, J. Daniels, D. E. Mittelberger, S. S. Bulanov, J.-L. Vay, C. G. R. Geddes, and E. Esarey, Phys. Rev. Lett. **113**, 245002 (2014).
[15] L. M. Chen, J. Zhang, Y. T. Li, H. Teng, T. J. Liang, Z. M. Sheng, Q. L. Dong, L. Z. Zhao, Z. Y. Wei, and X. W. Tang, Phys. Rev. Lett. **87**, 225001 (2001).
[16] Y. T. Li, J. Zhang, L. M. Chen, Y. F. Mu, T. J. Liang, Z. Y. Wei, Q. L. Dong, Z. L. Chen, H. Teng, S. T. Chun-Yu, W. M. Jiang, Z. J. Zheng, and X. W. Tang, Phys. Rev. E **64**, 046407 (2001).
[17] Y. T. Li, X. H. Yuan, M. H. Xu, Z. Y. Zheng, Z. M. Sheng, M. Chen, Y. Y. Ma, W. X. Liang, Q. Z. Yu, Y. Zhang, F. Liu, Z. H. Wang, Z. Y. Wei, W. Zhao, Z. Jin, and J. Zhang, Phys. Rev. Lett. **96**, 165003 (2006).
[18] H. Habara, K. Adumi, T. Yabuuchi, T. Nakamura, Z. L. Chen, M. Kashihara, R. Kodama, K. Kondo, G. R. Kumar, L. A. Lei, T. Matsuoka, K. Mima, and K. A. Tanaka, Phys. Rev. Lett. **97**, 095004 (2006).
[19] A. G. Mordovanakis, J. Easter, N. Naumova, K. Popov, P.-E. Masson-Laborde, B. Hou, I. Sokolov, G. Mourou, I. V. Glazyrin, W. Rozmus, V. Bychenkov, J. Nees, and K. Krushelnick, Phys. Rev. Lett. **103**, 235001 (2009).
[20] Y. Tian, J. Liu, W. Wang, C. Wang, A. Deng, C. Xia, W. Li, L. Cao, H. Lu, H. Zhang, Y. Xu, Y. Leng, R. Li, and Z. Xu, Phys. Rev. Lett. **109**, 115002 (2012).
[21] J. Y. Mao, L. M. Chen, X. L. Ge, L. Zhang, W. C. Yan, D. Z. Li, G. Q. Liao, J. L. Ma, K. Huang, Y. T. Li, X. Lu, Q. L. Dong, Z. Y. Wei, Z. M. Sheng, and J. Zhang, Phys. Rev. E **85**, 025401 (2012).
[22] W. Wang, L. Chen, J. Mao, K. Huang, Y. Ma, J. Zhao, L. Zhang, W. Yan, D. Li, J. Ma, Y. Li, X. Lu, Z. Wei, Z. Sheng, and J. Zhang, High Energy Density Physics **9**, 578 (2013).
[23] K. Estabrook and W. L. Kruer, Phys. Rev. Lett. **40**, 42 (1978).
[24] F. Brunel, Phys. Rev. Lett. **59**, 52 (1987).
[25] L. Chen, J. Zhang, Q. Dong, H. Teng, T. Liang, L. Zhao, and Z. Wei, Physics of Plasmas **8**, 2925 (2001).
[26] W. Kruer and K. Estabrook, Physics of Fluids **28**, 430 (1985).
[27] Z.-M. Sheng, K. Mima, Y. Sentoku, M. S. Jovanović, T. Taguchi, J. Zhang, and J. Meyer-ter Vehn, Phys. Rev. Lett. **88**, 055004 (2002).
[28] M. Thevenet, A. Leblanc, S. Kahaly, H. Vincenti, A. Vernier, F. Quere, and J. Faure, Nature Physics **12**, 355 (2016).
[29] J. Y. Mao, L. M. Chen, K. Huang, Y. Ma, J. R. Zhao, D. Z. Li, W. C. Yan, J. L. Ma, M. Aeschlimann, Z. Y. Wei, and J. Zhang, Applied Physics Letters **106**, 131105 (2015).
[30] A. Pukhov, Z.-M. Sheng, and J. M. ter Vehn, Physics of Plasmas **6**, 2847 (1999).
[31] C. Gahn, G. D. Tsakiris, A. Pukhov, J. Meyer-ter Vehn, G. Pretzler, P. Thirolf, D. Habs, and K. J. Witte, Phys. Rev. Lett. **83**, 4772 (1999).
[32] S. P. D. Mangles, B. R. Walton, M. Tzoufras, Z. Na-

jmudin, R. J. Clarke, A. E. Dangor, R. G. Evans, S. Fritzler, A. Gopal, C. Hernandez-Gomez, W. B. Mori, W. Rozmus, M. Tatarakis, A. G. R. Thomas, F. S. Tsung, M. S. Wei, and K. Krushelnick, Phys. Rev. Lett. **94**, 245001 (2005).

[33] S. Kneip, S. R. Nagel, C. Bellei, N. Bourgeois, A. E. Dangor, A. Gopal, R. Heathcote, S. P. D. Mangles, J. R. Marquès, A. Maksimchuk, P. M. Nilson, K. T. Phuoc, S. Reed, M. Tzoufras, F. S. Tsung, L. Willingale, W. B. Mori, A. Rousse, K. Krushelnick, and Z. Najmudin, Phys. Rev. Lett. **100**, 105006 (2008).

[34] Y. Y. Li, Y. J. Gu, Z. Zhu, X. F. Li, H. Y. Ban, Q. Kong, and S. Kawata, Physics of Plasmas **18**, 053104 (2011).

[35] X. Zhang, V. N. Khudik, and G. Shvets, Phys. Rev. Lett. **114**, 184801 (2015).

[36] T. W. Huang, A. P. L. Robinson, C. T. Zhou, B. Qiao, B. Liu, S. C. Ruan, X. T. He, and P. A. Norreys, Phys. Rev. E **93**, 063203 (2016).

[37] L. Willingale, P. M. Nilson, A. G. R. Thomas, J. Cobble, R. S. Craxton, A. Maksimchuk, P. A. Norreys, T. C. Sangster, R. H. H. Scott, C. Stoeckl, C. Zulick, and K. Krushelnick, Phys. Rev. Lett. **106**, 105002 (2011).

[38] L. Willingale, A. G. R. Thomas, P. M. Nilson, H. Chen, J. Cobble, R. S. Craxton, A. Maksimchuk, P. A. Norreys, T. C. Sangster, R. H. H. Scott, C. Stoeckl, C. Zulick, and K. Krushelnick, New Journal of Physics **15**, 025023 (2013).

[39] H. Alfvén, Phys. Rev. **55**, 425 (1939).

[40] I. Y. Dodin and N. J. Fisch, Physics of Plasmas **13**, 103104 (2006).

[41] Y. Sentoku, H. Ruhl, K. Mima, R. Kodama, K. Tanaka, and Y. Kishimoto, Physics of Plasmas **6**, 2855 (1999).

[42] W. L. Kruer, *The Physics of Laser Plasma Interactions* (Addison-Wesley, 1988).

[43] B. Liu, H. Y. Wang, J. Liu, L. B. Fu, Y. J. Xu, X. Q. Yan, and X. T. He, Phys. Rev. Lett. **110**, 045002 (2013).

[44] E. Esarey, C. B. Schroeder, and W. P. Leemans, Rev. Mod. Phys. **81**, 1229 (2009).

[45] M. Tzoufras, W. Lu, F. S. Tsung, C. Huang, W. B. Mori, T. Katsouleas, J. Vieira, R. A. Fonseca, and L. O. Silva, Phys. Rev. Lett. **101**, 145002 (2008).

[46] M. Tabak, J. Hammer, M. Glinsky, W. Kruer, S. Wilks, J. Woodworth, E. Campbell, M. Perry, and R. Mason, Physics of Plasmas **1**, 1626 (1994), 35th Annual Meeting of the Division-of-Plasma-Physics of the American-Physical-Society, St Louis, MO, Nov 01-05, 1993.

[47] K. A. Tanaka, T. Yabuuchi, T. Sato, R. Kodama, Y. Kitagawa, T. Takahashi, T. Ikeda, Y. Honda, and S. Okuda, Review of Scientific Instruments **76**, 013507 (2005).

[48] J. F. Briesmeister, *MCNP: A General Monte Carlo N-Particle Transport Code* (Los Alamos National Laboratory Report No. LA-13709-M, 2000).

[49] B. R. Maddox, H. S. Park, B. A. Remington, N. Izumi, S. Chen, C. Chen, G. Kimminau, Z. Ali, M. J. Haugh, and Q. Ma, Review of Scientific Instruments **82**, 023111 (2011).

[50] T. D. Arber, K. Bennett, C. S. Brady, A. Lawrence-Douglas, M. G. Ramsay, N. J. Sircombe, P. Gillies, R. G. Evans, H. Schmitz, A. R. Bell, and C. P. Ridgers, Plasma Physics and Controlled Fusion **57**, 1 (2015).

[51] R. Ramis, J. M. ter Vehn, and J. Ramrez, Computer Physics Communications **180**, 977 (2009).